J Electroceram (2009) 22:405–415
DOI 10.1007/s10832-008-9445-y

Heterogeneously doped nanocrystalline ceria films by grain boundary diffusion: Impact on transport properties

Scott J. Litzelman · Roger A. De Souza · Benjamin Butz · Harry L. Tuller · Manfred Martin · Dagmar Gerthsen

Received: 3 August 2007 / Accepted: 12 February 2008 / Published online: 5 March 2008

Abstract Heterogeneous doping of nanocrystalline ceria films, by controlled in-diffusion along grain boundaries, is explored as a means for modifying the space charge potential and the inhomogeneous distribution of defects in the space charge layer known to control the electrical properties of nanocrystalline electroceramics. Nanocrystalline cerium oxide thin films were grown by pulsed laser deposition and modified by a novel doping technique. Thin diffusion sources were deposited and cations such as Ni^{2+} and Gd^{3+} were in-diffused at temperatures of 700–800 °C along columnar grain boundaries normal to the surface; the resulting diffusion profiles were examined by Time-of-Flight SIMS. The properties of these modified films were compared with as-deposited samples, with in-diffusion resulting in decreased electrical conductivity. It is proposed that the variation in conductivity results from a redistribution of charge carriers in the space charge layers due to a change in the space charge potential.

Keywords Nanoionics · Cerium oxide · Grain boundary diffusion · Space charge

S. J. Litzelman (✉) · H. L. Tuller
Department of Materials Science and Engineering,
Massachusetts Institute of Technology,
Cambridge, MA 02139, USA
e-mail: sjlitzel@mit.edu

R. A. De Souza · M. Martin
Institute for Physical Chemistry, RWTH Aachen University,
52056 Aachen, Germany

B. Butz · D. Gerthsen
Laboratory for Electron Microscopy, Universität Karlsruhe (TH),
76128 Karlsruhe, Germany

1 Introduction

In the fields of solid state ionics and electroceramics, there is a continuing need for high temperature materials with superior properties for applications such as energy conversion, oxygen separation, and gas sensing. Depending on the application, high ionic and/or electronic conductivity is one such desired property. It is understood that interfacial structures, such as surfaces, grain boundaries, and second phases, can have a large impact on charge transport due to space charge effects [1]. Thus the logical extension of grain size down to the nanometer regime, in which the fractional density of interfaces is significantly enhanced, has led to unique properties changes not observed in the bulk [2, 3].

Doped cerium oxide is widely studied as a potential electrolyte for intermediate-temperature solid oxide fuel cells and oxygen permeation membranes [4, 5], as the introduction of acceptor ions on the Ce^{4+} site leads to the formation of oxygen vacancies with high mobility [6]. This combined with the high solubility for acceptors such as Y^{3+} and Gd^{3+}, leads to ceria's high ionic conductivity [7]. Nominally undoped ceria, while not as widely considered for technological applications, is of prime importance as a model system for studies that probe the effects of nanocrystalline dimensions on ionic and electronic transport. Indeed, over the past ten years, much work has been undertaken to develop a deeper understanding of the effects of nanocrystalline dimensions on the properties of ceria [8–13].

Chiang and co-workers [8] first observed that the decrease from microcrystalline to nanocrystalline grain sizes was accompanied by two distinct changes in the electrical conductivity. First, the conductivity of the nanocrystalline samples was found to be approximately two orders of magnitude higher. Second, the nanocrystalline

samples showed a negative pO_2 dependence resembling an n-type semiconductor, whereas the microcrystalline samples with identical composition showed no pO_2 dependence, indicative of an oxygen vacancy dominant regime controlled by compensating acceptor impurities. These observations were later quantitatively described by Tschöpe [12] and Kim [13] within the context of the space charge model. Namely, it was found that the natural occurrence of a positive space charge potential in the grain boundary core was compensated by a space charge layer enhanced in negative defects (electrons) and highly depleted of positive defects (oxygen vacancies). This combination of experimental data and analytical modeling serves as one of the best-understood examples of nanocrystalline effects on charge transport in a mixed ionic–electronic conducting (MIEC) electroceramic material to date.

In this work, a new approach is taken: the attempt to *control* nanoscale effects by influencing the space charge potential that exists at grain boundaries in ceria by heterogeneous doping, achieved via controlled in-diffusion along grain boundaries. As mentioned above, the space charge potential in ceria is normally of positive polarity, with magnitudes of approximately 0.3 [13] to 0.5 V [12] having been reported. There remains some discussion regarding the physical origin of this positive potential, but it has been proposed [14] based on computer simulations [15] that the energy of formation for an oxygen vacancy at a surface-like structure such as a grain boundary will be reduced compared to the corresponding energy in the bulk, due to a weakened bonding state. According to the space charge model, the core charge is compensated on both sides of the boundary by space charge regions of opposite polarity. In the Mott-Schottky approximation to Poisson's equation [16, 17], the width of the space charge layer λ^* is given as:

$$\lambda^* = \lambda\sqrt{\frac{4e}{k_B T}\Delta\phi(0)} \tag{1}$$

where e is the elementary charge, k_B, the Boltzmann constant, $\Delta\phi$ (0) the space charge potential in the grain boundary core, and λ the Debye length given by:

$$\lambda = \left(\frac{\varepsilon k_B T}{2z^2 e^2 c_\infty}\right)^{1/2} \tag{2}$$

where ε is the dielectric constant, z is the charge magnitude, and c_∞ is the bulk defect concentration. Thus, under conditions where ionized acceptors cannot redistribute in the space charge region, the width of the space charge region itself is dependent on the space charge potential. The equilibrium condition is given by the constancy of the electrochemical potential, $\tilde{u}_j = \mu_j + z_j e\varphi$ where μ_j and φ are the chemical and electrostatic potentials, respectively. This leads to a concentration profile given by:

$$\frac{c_j(x)}{c_{j\infty}} = \exp\left(-\frac{z_j e}{k_B T}\Delta\phi(x)\right) \tag{3}$$

where $\Delta\varphi(x)$ is the potential difference at a distance x from the boundary, relative to the bulk. Clearly, the larger the space charge potential, the larger the enhancement/depletion effects relative to the bulk. A change of the polarity of the space charge potential in the grain boundary core would, by necessity, lead to an inversion of charge carriers in the space charge layer. To systematically control such an effect is not trivial, given the complexity and distribution of various grain boundary structures, as well as the unique thermodynamics that govern these interfacial regions [18].

Recently, Avila-Paredes and Kim reported the effects of the addition of a small concentration (~ 0.5 cat %) of transition metal cations, by a solid state synthesis route, on the properties of bulk microcrystalline $Ce_{0.99}Gd_{0.01}O_{2-x}$ (CGO) [19]. It was observed that, while the transition metal addition had no effect on charge transport through the bulk, the addition of cations such as Co and Fe led to a tenfold decrease of the grain boundary resistivity. The authors found that the impurities segregated to triple point junctions and reported that the space charge potential decreased by as much as 20% in the case of Fe. This was attributed to the introduction of negative charge into the grain boundary core in the form of ionized acceptors.

In this study, grain boundary effects on conductivity are studied in nanocrystalline ceria *thin films*. Modification of grain boundaries is achieved by a *heterogeneous doping* technique consisting of precisely controlled in-diffusion of dopant ions along grain boundaries in the relatively low annealing temperature range of 700–800 °C. Thin films were selected as model systems because systematic and reproducible control of the microstructure, morphology, and properties of thin films can be achieved through the variation of deposition parameters such as temperature, oxygen working pressure, and laser repetition rate [20]. Further, given short diffusion lengths, they allow for the systematic control of grain boundary chemistry by in-diffusion.

2 Experimental

A nominally undoped cerium oxide pulsed laser deposition (PLD) target was prepared from cerium oxide powders (Alfa Aesar, 99.99%). The target was prepared by uniaxial pressing at 52 MPa followed by cold isostatic pressing at 275 MPa. The compact was sintered at 1425 °C for 5 h. The ceria films were deposited on (100) MgO and R-plane sapphire single crystal substrates (MTI Crystal) by PLD. A KrF eximer laser, emitting at 248 nm (Coherent COMPex

Pro 205), was used at an energy between 300–400 mJ/pulse with a repetition rate ranging from 12 to 25 Hz. The temperature of deposition was 700 °C and the oxygen working pressure ranged from 0.67 to 2.67 Pa in the deposition chamber. After deposition and before cooling, the oxygen pressure in the chamber was increased to approximately 670 Pa to facilitate more complete oxidation of the films.

Following deposition, the physical film properties were characterized by a Rigaku RU300 X-ray diffractometer (XRD), a FEI/Philips XL30 environmental scanning electron microscope (E-SEM), and Digital Instruments Nanoscope IIIa atomic force microscope (AFM). Further microstructural characterization was performed using a 200 keV Philips CM200 FEG/ST transmission electron microscope (TEM) equipped with a field emission gun and a 2k × 2k CCD camera. Energy dispersive X-ray spectrometry (EDX) was carried out by means of a NORAN Vantage system with a Ge X-ray detector using a probe diameter of about 1 nm. Electron energy loss spectroscopy (EELS) was performed utilizing a 200 keV Zeiss 922 microscope, equipped with an OMEGA energy filter. Cross-section as well as plan-view TEM samples were prepared by standard preparation procedures, including mechanical grinding, dimpling, polishing, and Ar^+ -ion milling (Gatan Duo mill, 2–4 keV, 12–20°). After preparation, a thin layer of carbon was deposited on the samples, except on the thin region of interest, in order to reduce charging effects in the electron microscope.

The ceria thin films were modified by depositing a thin, 20 nm diffusion source film on the surface. NiO films were formed by reactive sputtering from a Ni metal target in an oxygen pressure of 1.3 Pa. Gd_2O_3 films were deposited by electron-beam evaporation. These diffusion source/ceria samples were then annealed in air at temperatures from 700 to 800 °C in order to in-diffuse the source cations into the ceria layers. Diffusion profiles of several ceria samples of approximately 1 μm thickness modified with the NiO source were analyzed by Time-of-Flight Secondary Ion Mass Spectrometry (ToF-SIMS). Typically, 25 keV Ga^+ ions raster scanned over (100×100 μm) were used to generate secondary ions; 1 keV O_2^+ ions raster scanned over (300× 300 μm) were used for sputter etching of the surface. A low energy beam of electrons was used for charge compensation. Positive secondary ions arising from the diffusion source as well as from the substrate were monitored; short-circuiting effects due to pinholes were removed by generating 2D ion maps for each sample and defining regions-of-interest only were ion concentrations were laterally homogeneous. Additional information regarding the SIMS technique and instrument can be found in the literature [21, 22].

Electrical characterization was performed on as-deposited and modified films of approximately 140–200 nm thickness on MgO substrates. In the case of the films modified by Ni in-diffusion, the diffusion source was removed by reducing NiO to Ni in 95:5 N_2/H_2 gas, followed by etching in a solution of 3:1 HNO_3:H_2O, leaving only the ceria layer on the surface. Removal of the source film was observed visually and confirmed by XRD. Dense interdigitated microelectrodes were prepared by a photolithographic lift-off process (NR7 photoresist, Futurex). A 10 nm Ti adhesion layer and 115 nm Pt layer were deposited by sputtering on top of the photoresist and ceria layer. The photoresist was then removed by soaking in acetone. The finger width and inter-electrode spacing were 40 and 50 μm. The samples were measured from 300–600 °C in an open-air microprobe station (Karl Suss) and a custom-designed enclosed probe station, manufactured by McAllister Technical Services (Coeur d'Alene, ID). This enclosed probe station was fitted with a heating stage and a gas flow system capable of varying the oxygen partial pressure in the chamber. Electrical measurements were made in-plane via two-point DC measurements (HP 4142B) and impedance spectroscopy (Solartron 1260) in the frequency range of 10 MHz to 1 Hz (50 mV AC amplitude).

3 Results

3.1 Film characterization

An XRD scan of a sample grown on single crystal MgO is found in Fig. 1. The film shows a preferred orientation matching that of the substrate, though smaller (111) and (311) reflections were at times also observed. The degree of

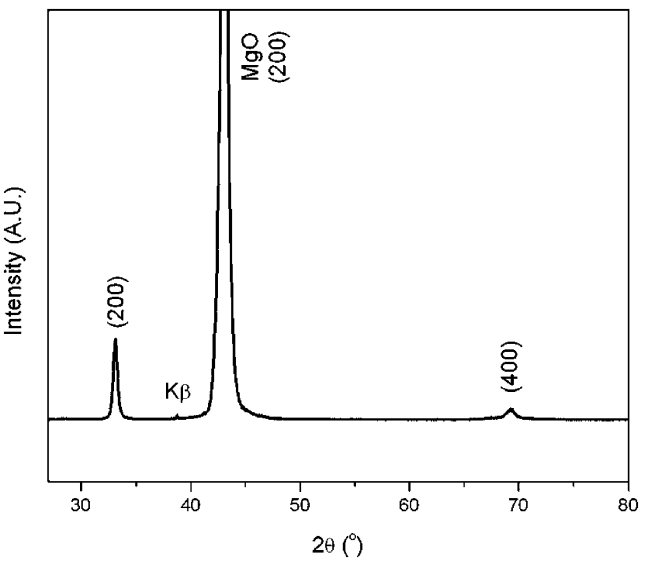

Fig. 1 XRD pattern of CeO_2 on MgO. The pattern indicates preferred (100) orientation. Evidence of (111) and (311) reflections was also found in several samples

preferred orientation is strongly dependent on deposition temperature, and while the target deposition temperature remained constant at 700 °C, minor fluctuations between different samples may have led to small changes in the degree of preferred orientation. XRD data of ceria films grown on sapphire display a very similar degree of preferred (100) orientation. The as-deposited films appear crack-free and dense.

An AFM micrograph of the ceria surface can be seen in Fig. 2. The ceria surface is extremely flat, with a root mean square surface roughness of approximately 1 nm. The grain sizes are on the order of 25–40 nm and are relatively monodisperse in nature. This is confirmed by multiple AFM scans of several samples and is quite consistent. The film microstructure was also examined by SEM. Samples were scribed lightly on the backside and then cleaved. A sample cross section can be seen in Fig. 3. This cross section appears to be consistent with the authors' intended goal of a columnar microstructure. However, it must be reiterated that this micrograph is of a fracture cross section, and thus may not be completely indicative of the true microstructure.

To further analyze this morphology, cross sectional TEM measurements were made. The bright field micrograph (a) with corresponding dark field micrograph (b), presented in Fig. 4, display a columnar microstructure through the thickness of the film. The interface between the MgO substrate and the ceria film is marked by the dashed line. A high resolution TEM micrograph (HRTEM) is shown in Fig. 5 for a sample annealed with Ni at 650 °C for 10 h. While the grain in the left side of the image is aligned close to a (112) zone axis, the second grain is oriented in a (111) two-beam condition. The grain boundary is marked by

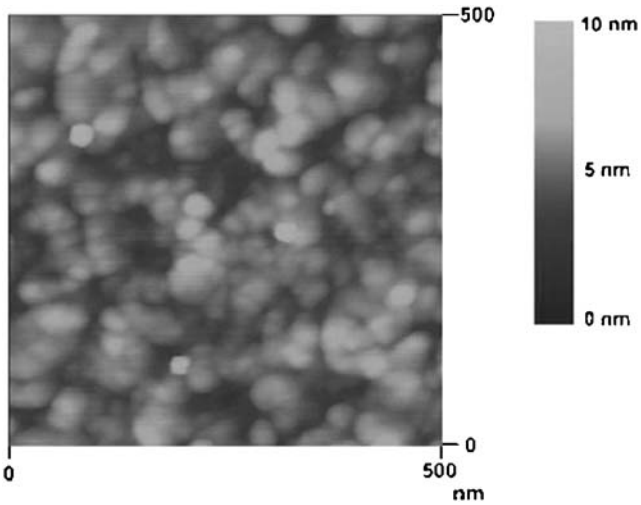

Fig. 2 AFM scan of the ceria surface. As-deposited grain sizes are on the order of 25–40 nm and the R.M.S. surface roughness is less than 1 nm

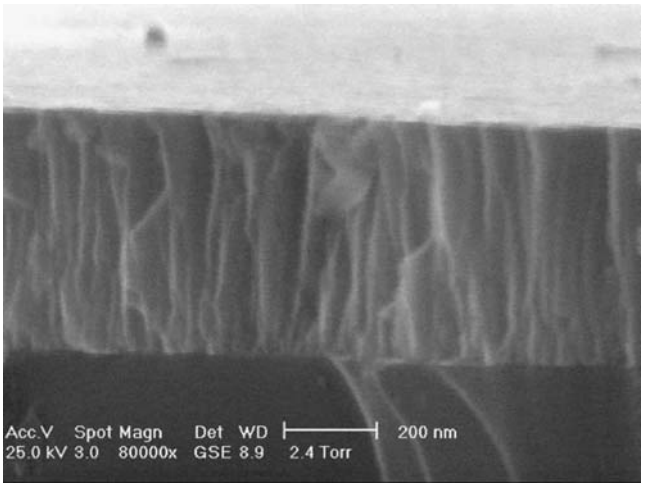

Fig. 3 Cross sectional environmental SEM image of as-deposited ceria layer

arrows. This figure reveals two key pieces of information regarding the grain boundary structure in the investigated samples: the grain boundary is relatively sharp in spatial extent (no broad amorphous layer) and no second phase, either glassy or precipitated Ni, is detected.

3.2 Cation in-diffusion

ToF-SIMS depth profiles for Ni resulting from the annealing of 20 nm NiO/1100 nm ceria samples are shown in Fig. 6 in the form of log (normalized intensity) versus depth. The as-deposited specimen exhibits an apparent penetration to a depth of ~300 nm into the ceria layer, but this profile is most likely not due to Ni diffusion. The origin of this feature is unclear, but given the room temperature deposition of the source film and the relative intensities of the as-deposited and annealed profiles, this feature has little effect on the analysis. The profile for a specimen, following an anneal at 700 °C for 5 h, shows a clear diffusion profile that resembles a simple error function solution to Fick's Second Law. This signal is well above the noise of the measurement, and all profiles were measured at least twice on the same sample to ensure consistency. The signal also decays to the point of no detection before reaching the single crystal substrate, which begins approximately at a depth of 1,175 nm. This indicates that Ni has diffused through most, yet not the entire ceria layer. A profile is also shown for a specimen following an anneal at 800 °C for 5 h. Here, the initial concentration in the upper portion of the ceria layer is consistent with the 700 °C data, but the profile shows a constant level of penetration down to the substrate interface, indicating that Ni has diffused through the entire layer. Continued annealing at 800 °C for longer periods of time such as 10 h results in a profile nearly identical to the one at 5 h.

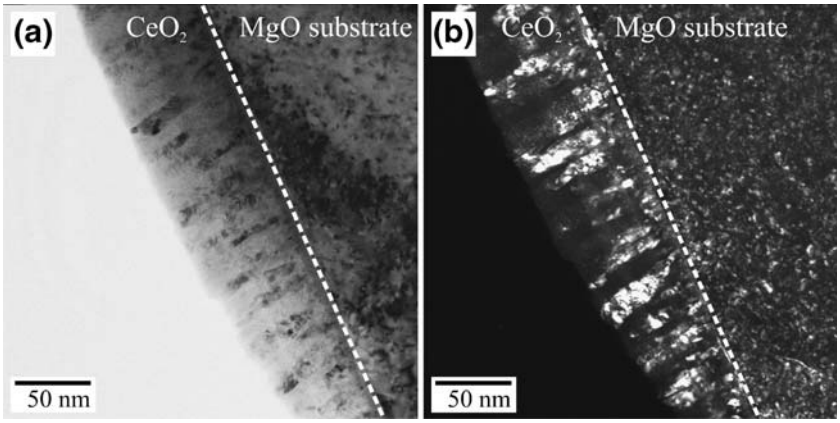

Fig. 4 (**a**) Bright field micrograph and (**b**) dark field micrograph from a TEM cross section of the ceria layer deposited on MgO, indicating a columnar microstructure through the thickness of the film

In addition to cations originating from the diffusion source, substrate cations were monitored as well. Figure 7 demonstrates the diffusion of Mg out of the MgO substrate. The as-deposited signal shows essentially no diffusion, but the profile after annealing at 700 °C for 5 h indicates that diffusion into part of the ceria layer has taken place; penetration of approximately 300 nm is observed before the profile becomes flat. The general shape of the Mg profile resembles the Ni profile at 700 °C, and these profiles are analyzed quantitatively below.

3.3 Electrical characterization

A sample impedance spectroscopy Nyquist plot is shown in Fig. 8. Consistent with previous reports for nanocrystalline ceria [9, 13] only a single semicircle is evident in this plot. Conductivity values calculated from two-point DC I-V sweeps from −0.15 V to + 0.15 V are consistent with the low frequency intercept of the impedance plots, indicating no appreciable impedance resulting from the Ti/Pt electrodes. The Arrhenius plot for the electrical conductivity of as-deposited and modified films is shown in Fig. 9. In order to indicate the relative error of the measurement, the data set labeled 'as-deposited' consists of several measurements on multiple samples with varying electrode spacing. There is an apparent change of activation energy from 0.70±0.21 to 1.04±0.11 eV at ~ 400 °C, possibly due to redox reactions that become kinetically favorable at elevated temperatures. The electrical conductivity of two films modified with Gd_2O_3 and NiO are also found in Fig. 9. The conductivity decreases by more than an order of magnitude, yet the activation energies for temperatures of 400 °C and above, 0.99±0.14 and 1.04±0.08 eV for Gd_2O_3 and NiO doping respectively, show no significant change relative to the undoped specimens.

In addition, several samples were annealed under the same conditions as the modified samples, but with no diffusion source. In Fig. 9, the data for films annealed in air at 600 °C for 5 h and 800 °C for 20 h also show a conductivity decrease, though considerably less than that of the modified films. AFM analysis of post-annealed (800 °C) samples indicates some grain growth, as the mean grain size

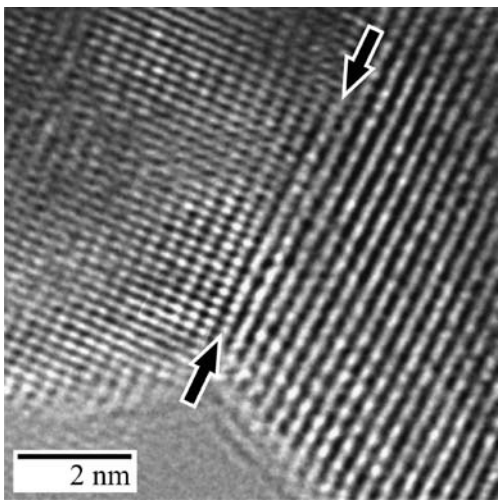

Fig. 5 HRTEM micrograph of a grain boundary in CeO_2 annealed in the presence of Ni at 650 °C for 10 h

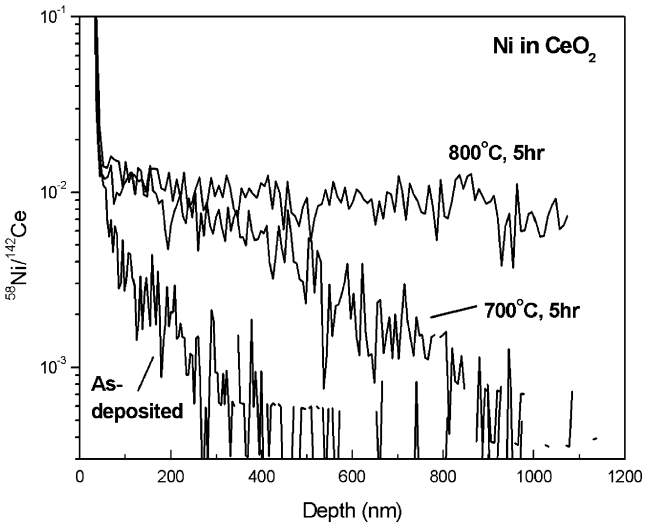

Fig. 6 SIMS spectra of NiO/ceria films with no anneal, as well as heating at 700 and 800 °C for 5 h. The ^{58}Ni signal is normalized by ^{142}Ce

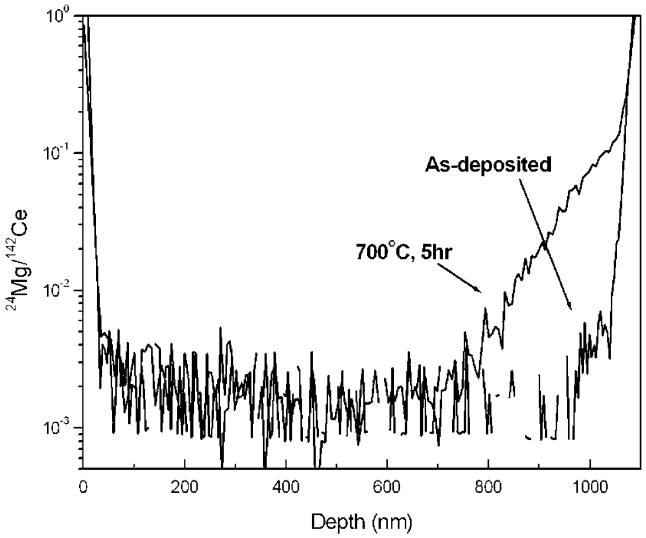

Fig. 7 SIMS spectra of Mg diffusing out of the substrate and into the ceria layer with no anneal, as well as heating at 700 °C for 5 h. The ^{24}Mg signal is normalized by ^{142}Ce

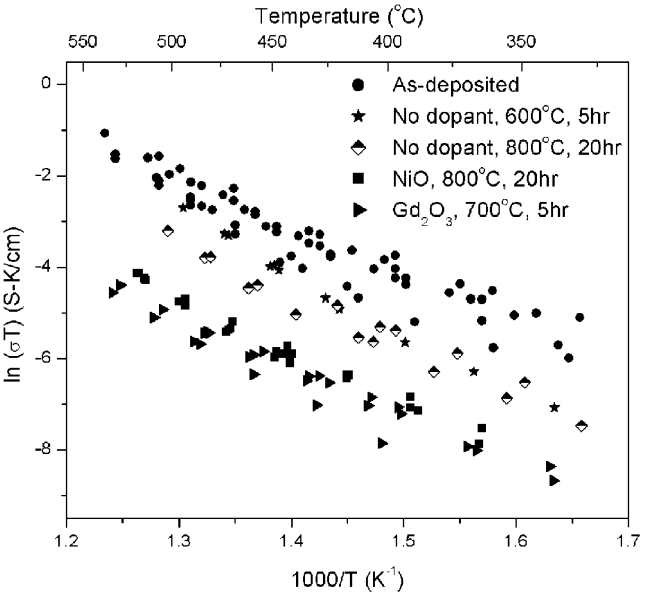

Fig. 9 Arrhenius plot of the electrical conductivity of as-deposited and modified ceria thin films. Annealing with no diffusion source results in a decrease in the electrical conductivity, and annealing in air with a NiO or Gd_2O_3 diffusion source results in a greater decrease in the conductivity

increases by approximately a factor of two. The pO_2 dependence of the conductivity is shown in Fig. 10. The as-deposited film shows a slope of −0.21±0.02, indicative of electron-dominated transport, in good agreement with literature data for nanocrystalline ceria [8, 9]. The film modified with NiO at 800 °C shows a clear conductivity decrease; however, the pO_2 dependence of −0.23±0.04 shows no clear statistical difference at the 95% confidence level.

4 Discussion

In order to allow for a conclusive evaluation of the effects of grain boundary doping by in-diffusion, first the properties of the as-deposited thin films were studied in detail. A key feature relevant to the successful heterogeneous doping of ceria was the ability to reproducibly grow nanocrystalline, columnar ceria thin films. The combination of AFM, SEM and TEM (Figs. 2, 3 and 4) indicates clearly that the films are both nanocrystalline, with initial grain sizes of approximately 25–40 nm, and of a columnar microstructure throughout the thickness of the film. The implication of these features is that a high cross-section of grain

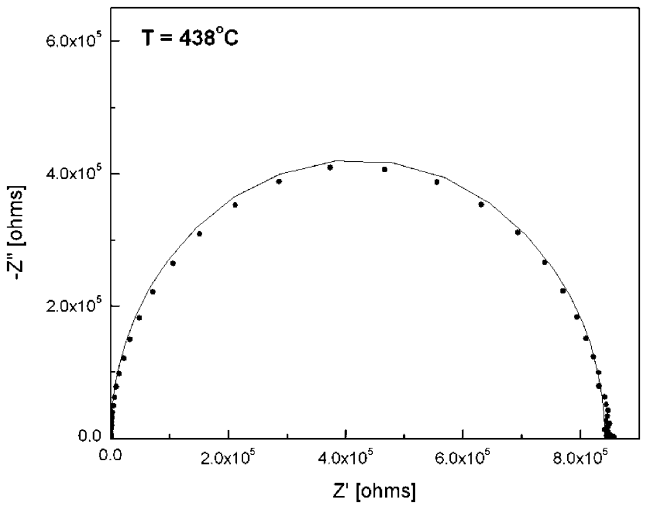

Fig. 8 Sample impedance spectroscopy Nyquist plot of nanocrystalline ceria measured at 438 °C in air. Only one semicircle is evident, consistent with literature data

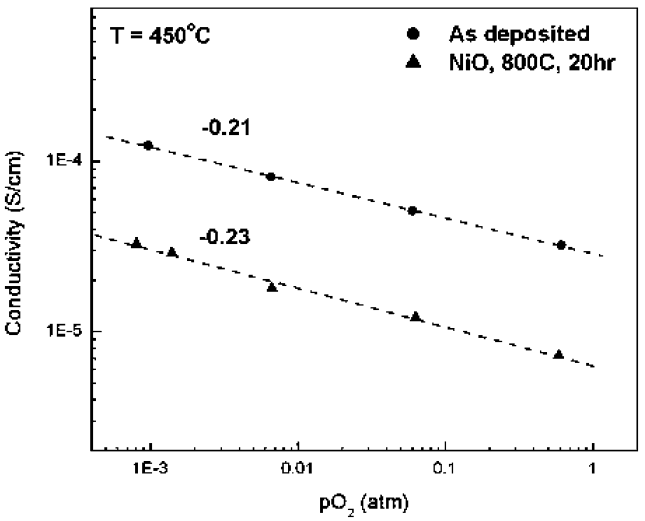

Fig. 10 Oxygen partial pressure dependence of the electrical conductivity, measured at 450 °C. Both as-deposited films and ones annealed at 800 °C for 20 h in air show essentially the same slope, indicating a consistent conduction mechanism. The conductivity of the modified sample was decreased by almost an order of magnitude

boundaries lies normal to the surface of the film, creating many parallel fast diffusion pathways for ions to migrate along. Figure 5 shows that no amorphous regions or second phases were detected along the grain boundaries, even after annealing in the presence of a diffusion source.

Several important features can be gleaned from the diffusion profiles in Figs. 6 and 7. The diffusion profiles of both Ni and Mg at 700 °C are similar in shape and indicate only one diffusion mechanism. The vast majority of diffusion studies on polycrystalline materials report behavior in the Harrison regime 'B' [23] which consists of the convolution of two transport mechanisms: bulk and grain boundary diffusion. The typical approach followed in this case is the method of LeClaire [24], in which the bulk diffusivity is first found and then used to find the product of the grain boundary diffusivity and grain boundary width (δD_{GB}). Since the data in Figs. 6 and 7 bear no resemblance to the Harrison regime B, diffusion must occur in the Harrison regime A (homogeneous diffusion through bulk and grain boundaries) or C (diffusion exclusively along grain boundaries), both of which would result in a single apparent diffusion profile.

The authors believe that, given the literature data on cation diffusion in fluorites [25, 26], bulk diffusion is highly unlikely to occur to any appreciable degree in this relatively low temperature range. Sirman and co-workers [25] reported bulk diffusivity values for Co and Fe in bulk, microcrystalline $Ce_{0.9}Gd_{0.1}O_{1.95}$ on the order of 10^{-14} to 10^{-15} cm^2/s at 1250 °C; in this study, similar orders of magnitude, calculated and discussed below, are observed at 700 °C. Since grain boundary diffusion of cations is commonly many orders of magnitude faster than bulk diffusion in metal oxides [27, 28] and there is such a large cross-section of grain boundaries normal to the surface, it is reasonable to assume that the diffusion profiles result solely from a grain boundary mechanism, thus occurring in the Harrison regime C.

The boundary conditions to Fick's Second Law chosen in this study are that of a constant diffusion source. While this may at first appear counterintuitive given the very thin nature of the source film (20 nm) compared to the ceria layer (~1,100 nm), there are two experimental observations that support this choice. First, it can be seen in Fig. 6 that for Ni diffusion at 700 and 800 °C, the Ni levels near the surface remain relatively constant as a function of annealing conditions, and do not decrease as would a finite source. Second, under all annealing conditions, the ToF-SIMS depth profiles for the source layer show a constant thickness, indicating that the source is still present even after anneals of 800 °C for 10 h and is not consumed during the annealing process.

This latter point indicates that the amount of cations that has diffused in from the source is quite small, as the source film does not appear to change. Correspondingly, TEM cross section analyses with EDX and EELS, originally focused on the determination of the dopant distribution at grain boundaries, did not yield any detectable amount of Ni ions in the bulk or grain boundaries. This is ascribed to the electron-probe diameter of 1 nm compared to the small grain boundary width, which requires a significant Ni concentration in the grain boundaries to exceed the detection limit of the applied techniques. While the SIMS measurements reproducibly demonstrate that cation diffusion has indeed taken place, all other evidence suggests that the impurity concentrations are quite low. These observations lend further support to grain boundary diffusion as the prevailing mechanism.

The well-known solution to constant source boundary conditions is given by the complementary error function:

$$\frac{c(x,t)}{c_O} = erfc\left(\frac{x}{2\sqrt{Dt}}\right) + c_{BG} \tag{4}$$

where c_O is the surface concentration and c_{BG} is the background concentration, indicative of the detection limit for each species in the SIMS spectrum. The data fit of this model to the Ni profile at 700 °C is shown in Fig. 11. The fit of the data to the constant source solution is quite satisfactory, and the resulting value for D_{GB} is 4.6×10^{-14} cm^2/s. Unfortunately, the profile at 800 °C is flat and a precise value for the diffusivity cannot be found; in principle, a fit of the diffusion equation to the data is possible, but since the profile is flat, the results obtained would be unreliable. The only information that can be extracted is the minimum diffusion coefficient, which can be estimated via the diffusion length, $x = 2\sqrt{Dt}$; this calculation yields $D_{GB}(\text{min}) = 1.7\times10^{-13}$ cm^2/s at 800 °C

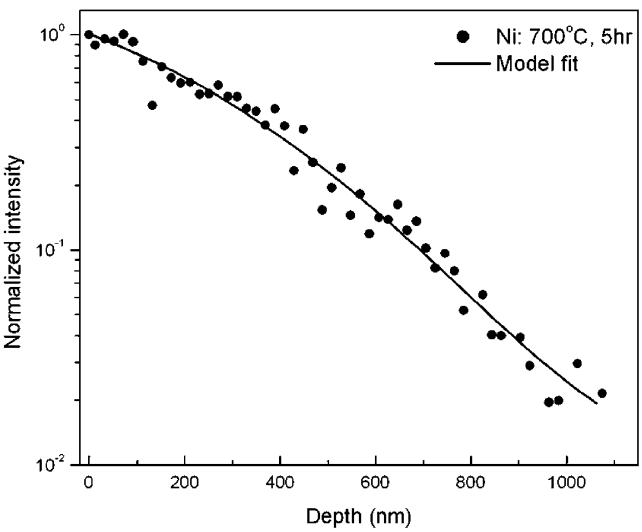

Fig. 11 Diffusion profile for Ni in ceria after annealing at 700 °C for 5 h (data points). The *solid line* corresponds to the fit to the constant source solution. $D_{GB} = 4.6\times10^{-14}$ cm^2/s

(based on $t=5$ h). It should be noted that this value is merely an estimate and that the actual diffusivity is likely higher. Using the same sample and method, the Mg diffusivity was found to be $D_{GB}=2.8\times10^{-15}$ cm^2/s at 700 °C, almost an order of magnitude lower than the diffusivity of Ni. The fit of the constant source model to the Mg profile is shown in Fig. 12 and is again satisfactory.

The results of the diffusion profiles (Figs. 6 and 7) and model fits (Figs. 11 and 12) for Ni and Mg in ceria at 700 °C are relevant from both a scientific and technological point-of-view. From the scientific standpoint, this represents, to the best of the authors' knowledge, the lowest temperatures at which cation diffusion coefficients have been measured in ceria. The combination of precisely controlled thin films with a very low surface roughness (even after annealing), a high-sensitivity analytical technique in ToF-SIMS, and annealing conditions in the Harrison regime C, allow for direct measurement of grain boundary diffusivities without prerequisite knowledge of the bulk diffusion coefficient and the grain boundary width. Accuracy is also enhanced by fitting the diffusion data with a single parameter.

From a technological point-of-view, these cation diffusivity values are many orders of magnitude lower than corresponding values for oxygen. However, it has been shown in degradation studies [29, 30] that the slowest species will be rate-determining and will control the lifetime and performance of solid state ionic devices, such as solid oxide fuel cells (SOFCs). The magnitudes of D_{GB} measured in this study, 10^{-14} to 10^{-15} cm^2/s, indicate that cations will diffuse hundreds of nanometers to a few microns along grain boundaries within a few hours at 700–800 °C. With the increasing interest in micro-SOFCs for portable power generation and reduced temperature operation [31, 32], there has been a strong incentive to markedly decrease the electrolyte thickness. As a consequence, cation grain boundary diffusion may represent a serious challenge to long-term reliability in this category of SOFCs and therefore deserves further investigation.

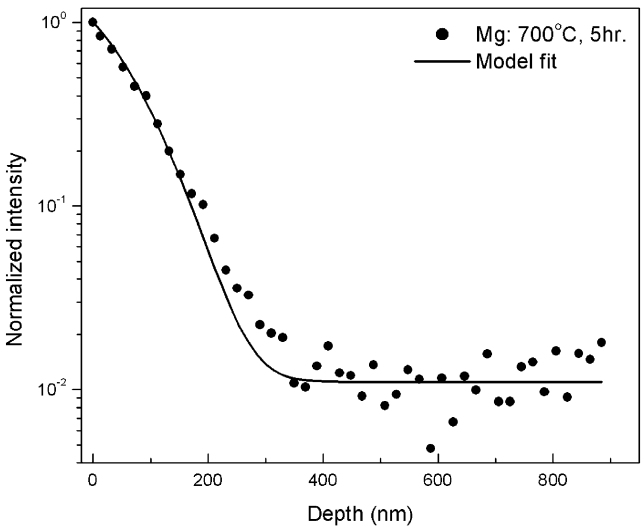

Fig. 12 Diffusion profile for Mg in ceria after annealing at 700 °C for 5 h (data points). The *solid line* corresponds to the fit to the constant source solution. $D_{GB}=2.8\times10^{-15}$ cm^2/s

The temperature and pO_2 dependence of the electrical conductivity of as-deposited and modified films also show interesting results. The activation energy below 400 °C, 0.70±0.21 eV, is higher than the accepted value for the small polaron hopping energy in bulk ceria, 0.4 eV [33], but lower than the activation energy seen at temperatures above 400 °C. At this time, the source of the change in activation energy around 400 °C is unclear. It may result from a partially frozen-in defect concentration in the bulk, as discussed by Sasaki and Maier [34, 35]. From Figs. 9 and 10, the high temperature thermal activation energy and the pO_2 dependence for the as-deposited samples were found to be 1.04±0.11 eV and −0.21±0.02, respectively. While the activation energy is lower than that reported in reference [9] (1.35 eV) and 13 (1.39 eV), it is in good agreement with reference [8]. Likewise, the pO_2 dependence is in good agreement with references [8, 9]. Both the activation energy and pO_2 dependence are indicative of electrons as the primary charge carrier in these films. Thus, the as-deposited films represent a well-understood baseline from which comparisons may effectively be made.

The magnitude of the as-deposited conductivity values are significantly increased relative to the corresponding electronic partial conductivity expected in bulk microcrystalline ceria. Using data from reference [33] and assuming a nominal acceptor concentration of 150 ppm, one calculates, at 500 °C, an electronic conductivity approximately four orders of magnitude lower than that reported in Fig. 9 in this study. This enhancement of electronic conductivity in nanocrystalline ceria has been reported in several previous studies [8, 9, 12, 13]. The conductivity data in Fig. 9 also demonstrates that annealing in the presence of a source of acceptor ions such as Ni^{2+} and Gd^{3+} results in a decrease in the conductivity by more than an order of magnitude. The conductivity values for Gd^{3+} doping at 700 °C for 5 h and Ni^{2+} doping at 800 °C for 20 h are similar in magnitude and slope. There are several physical phenomena that could lead to such conductivity decreases: (1) structural changes in the film such as grain growth, (2) acceptor doping in the bulk, and (3) alterations of the grain boundary (and thus space charge) properties. These three phenomena are discussed below.

Grain growth could lead to lower conductivity, as a smaller volume of each grain would be comprised of the electron-enhanced space charge region. Grain growth would thus dampen the effects of nanocrystallinity in ceria and in the limit of very large grain growth, would approach the properties of microcrystalline ceria as reported by

Chiang, et al. [8]. AFM measurements of samples, following annealing at 800 °C, do indicate some grain growth, with the mean grain size increasing by approximately a factor of two. As seen in Fig. 9, annealing without a diffusion source results in a decrease in the electrical conductivity by approximately a factor of 5 at 500 °C. These observations indicate that grain growth may indeed play a role in the conductivity change, though the decrease in conductivity is not sufficient to describe the total change evident in the presence of a diffusion source. In addition, Figs. 7 and 12 clearly demonstrate that even without a diffusion source on the ceria surface, cations from the substrate do migrate along the grain boundaries in this temperature range. Taken together, this data leads the authors to conclude that structural changes in the film such as grain growth may play a role in the conductivity behavior, but cannot by themselves explain the large conductivity decrease in the presence of dopants.

Another possible explanation for the observed trends is acceptor doping in the bulk. In the case of substitution of a trivalent dopant on a cerium site, the defect reaction would proceed as:

$$A_2O_3 \xrightarrow{CeO_2} 2A'_{Ce} + V_O^{\bullet\bullet} + 3O_O^x \tag{5}$$

in which A'_{Ce} is a trivalent substitutional acceptor, and $V_O^{\bullet\bullet}$ is a doubly ionized oxygen vacancy. Furthermore, the electron density, n, and oxygen vacancy concentration $\left[V_O^{\bullet\bullet}\right]$ are related via the reduction reaction:

$$O_O \overset{CeO_2}{\longleftrightarrow} V_O^{\bullet\bullet} + 2e' + 1/2O_2 \tag{6}$$

and the corresponding mass action reaction:

$$\left[V_O^{\bullet\bullet}\right] n^2 P_{O_2}^{1/2} = K_R(T) \tag{7}$$

in which P_{O_2} is the oxygen partial pressure and $K_R(T)$ is the equilibrium constant. This increase in the oxygen vacancy concentration leads to increasing ionic partial conductivity at the expense of the electronic partial conductivity (see Eq. 7). Since the mobility of oxygen vacancies is several orders of magnitude lower than that of electrons [33], this is expected to lead to a decrease of the total conductivity, which is indeed observed. However, in the discussion of cation in-diffusion above, the authors presented the case for grain boundary diffusion being the only process of mass transport occurring at this relatively low annealing range. Variations in electrical properties due to changes in acceptor density in the bulk are therefore unsupported.

It is therefore proposed that the observed conductivity decrease results from a change in the space charge potential in the grain boundary core. The diffusion of cations along the grain boundaries alters the grain boundary chemistry, and may contribute to a net increase in negative charge if incorporated substitutionally on Ce^{4+} sites. The partial compensation of the excess positive charge in the boundary core by the introduction of the acceptors would lead to a space charge potential that is still positive, but reduced in magnitude. The electron concentration in the space charge layer will be reduced but still dominant, and the oxygen vacancy concentration, as a doubly ionized defect, will increase more sharply than the electrons will decrease. This effect can be seen schematically in Fig. 13. Using established values for the reduction enthalpy in bulk ceria [33], sample profiles of electrons and oxygen vacancies were plotted for space charge potentials of +0.50 and +0.45 V respectively. These potentials were chosen because they are consistent with calculated values of the space charge potential with and without grain boundary modification by segregation [19]. According to Kim and Maier [13], the electrical conductivity of nanocrystalline ceria is best described by the Mott-Schottky model, as mentioned above. The concentration profiles in Fig. 13 were calculated as [16, 17]:

$$\frac{c_V(x)}{c_{V\infty}} = \exp\left[-\frac{1}{2}\left(\frac{x-\lambda*}{\lambda}\right)^2\right] \tag{8}$$

$$\frac{c_n(x)}{c_{n\infty}} = \exp\left[\left(\frac{x-\lambda*}{\lambda}\right)^2\right] \tag{9}$$

For the illustrated shift in potential of −50 mV, the electron concentration near the grain boundary core decreases by approximately 55% and the oxygen vacancy concentration increases by 400%. However, the oxygen vacancy concen-

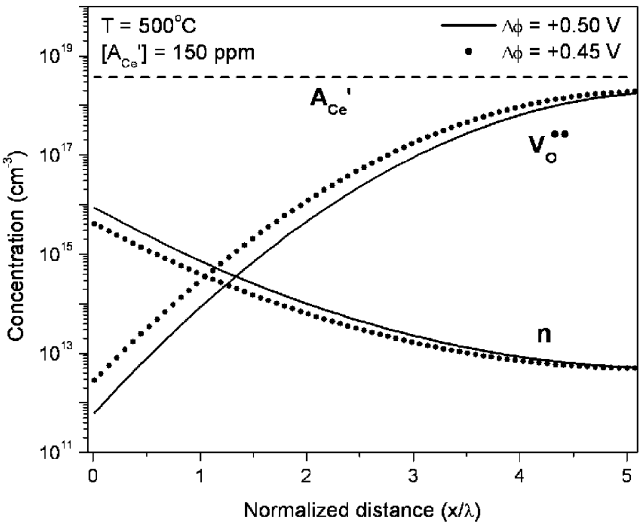

Fig. 13 Defect profiles in the space charge region under Mott-Schottky conditions. The concentrations of electrons and oxygen vacancies are calculated from data in reference [33] for space charge potentials of +0.50 V and +0.45 V. [A_{Ce}'] represents the concentration of a background acceptor impurity, such as La or Gd [9]

tration near the interface remains more than two orders of magnitude lower than the electrons. These model profiles are consistent with the hypothesis that the modified samples contain a reduced concentration of electrons in the space charge region, but that electronic conductivity remains the dominant contribution to the overall conductivity. As shown in reference [13], the temperature dependence of the electronic conductivity can be expressed as:

$$k_B \frac{\partial \ln \sigma_{el}}{\partial 1/T} = -E_{n\infty} + e\left(\Delta\phi(0) + \frac{1}{T}\frac{\partial \Delta\phi(0)}{\partial 1/T}\right) \qquad (10)$$

where $E_{n\infty}$ is the activation energy for electrons in bulk ceria. Using literature values of 2.37 for $E_{n\infty}$ [33] and 0.1 V for $(1/T)\partial\Delta\varphi(0)/\partial(1/T)$ [13], the activation energy for electronic conduction can be expected to increase by 2.8% with a 50 mV decrease in the space charge potential. The calculated activation energy for the NiO-modified sample was found to be the same as the as-deposited value, 1.04 eV. For a 95% confidence interval, the error bars for the as-deposited and NiO-modified data are ± 0.11 and 0.08 eV, respectively. Thus, the error bars associated with this confidence interval are too large to determine whether the expected increase in activation energy does or does not occur. Future systematic studies are being designed to enable one to correlate barrier height and the nature and concentration of the grain boundary dopant.

This hypothesis that Ni at the grain boundaries serves to reduce the barrier height is also consistent with the results of Avila-Paredes and Kim [19], who observed that the segregation of ions such as Fe and Co to triple point junctions in bulk microcrystalline $Ce_{0.99}Gd_{0.01}O_{2-x}$ led to a small decrease in the space charge potential (though still positive) and a decrease in the grain boundary resistivity. In that study, the authors attributed the reduced grain boundary resistivity to negative charges introduced by transition metal ions. This hypothesis is also consistent with all aspects of the experimental data in this study: diffusion only along grain boundaries and a conductivity decrease with no detectable change of predominant conduction mechanism, as measured by thermal activation and pO_2 dependence.

Additional work is underway, via blocking measurements, to determine the electronic and ionic partial conductivities of the as-deposited and modified samples. Assuming our hypothesis regarding the acceptor-induced reduction in the barrier potential height, a significant increase in ionic conductivity will be detected.

5 Summary

Nanocrystalline, columnar thin films of ceria were fabricated by PLD. Diffusion sources such as NiO and Gd_2O_3 were deposited and the cations were in-diffused in the temperature range of 700–800 °C. Depth profiles measured by ToF-SIMS reveal only one diffusion mechanism, attributed solely to grain boundary diffusion, thus falling within the Harrison regime C. Profiles of Ni and Mg were obtained following annealing at 700 °C, and the grain boundary diffusion coefficients were determined by use of the constant source solution to the diffusion equation; grain boundary diffusivities for Ni and Mg were found to be 4.6×10^{-14} and 2.8×10^{-15} cm^2/s, respectively. Cations may therefore diffuse via grain boundaries between several hundred nanometers and a few microns at operating conditions as low at 700 °C for several hours.

The modification of grain boundaries by the controlled in-diffusion of cations resulted in a decrease of the space charge potential due to the introduction of net negatively charged species into the grain boundary core. A decrease in the electrical conductivity, by more than one order of magnitude, without an apparent change in conduction mechanism was observed. This is attributed to a decrease of the space charge potential to a lower, yet still positive value which was compensated by a decrease in electron concentration and an increase in oxygen vacancy concentration in the space charge layer. While the modified films remain predominantly electronically conducting, the reduced electron concentration in the space charge layer leads to a macroscopic decrease in total conductivity in the nanocrystalline ceria thin films.

Acknowledgements RWTH Aachen University is gratefully acknowledged for providing a Charlemagne scholarship for a student visitation by S.L. This work was supported by the National Science Foundation under award DMR-0243993 and by the Deutsche Forschungsgemeinschaft under project Ge 841/18 within the framework of a joint DFG/NSF program.

References

1. J. Maier, Prog. Solid State Chem. **95**, 171 (1995)
2. J. Maier, Electrochemistry **68**, 395 (2000)
3. H.L. Tuller, Solid State Ion. **131**, 143 (2000)
4. H. Inaba, H. Tagawa, Solid State Ion. **83**, 1 (1996)
5. M. Mogensen, N.M. Sammes, G.A. Tompsett, Solid State Ion. **129**, 63 (2000)
6. J.A. Kilner, B.C.H. Steele, in *Nonstoichiometric Oxides*, ed. by O. T. Sorensen (Academic Press, New York, 1981)
7. H. Yahiro, K. Eguchi, H. Arai, Solid State Ion. **36**, 71 (1989)
8. Y.-M. Chiang, E.B. Lavik, I. Kosacki, H.L. Tuller, J. Ying, J. Electroceram. **1**, 7 (1997)
9. J.-H. Hwang, T.O. Mason, Z. Phys. Chem. **207**, 21 (1998)
10. T. Suzuki, I. Kosacki, H.U. Anderson, J. Am. Ceram. Soc. **85**(6), 1492 (2002)
11. A. Tschöpe, E. Sommer, R. Birringer, Solid State Ion. **139**, 255 (2001)
12. A. Tschöpe, Solid State Ion. **139**, 267 (2001)
13. S. Kim, J. Maier, J. Electrochem. Soc. **149**(10), J73 (2002)
14. J. Maier, Solid State Ion. **154–155**, 291 (2002)
15. T.X.T. Sayle, S.C. Parker, C.R.A. Catlow, Surface Science **316**, 329 (1984)

16. N.F. Mott, Proc. R. Soc. Lond. **171**, 27 (1939)
17. W. Scottky, Z. Phys. **113**, 367 (1939)
18. J. Maier, *Physical Chemistry of Ionic Materials* (Wiley & Sons, West Sussex, 2004)
19. H.J. Avila-Paredes, S. Kim, Solid State Ion. **177**, 3075 (2006)
20. C.V. Thompson, Annu. Rev. Mater. Sci. **30**, 159 (2000)
21. R.A. De Souza, J. Zehnpfennig, M. Martin, J. Maier, Solid State Ion. **176**, 1465 (2005)
22. R.A. De Souza, M. Martin, Phys. Status Solidi (c) **4**(6), 1785 (2007)
23. L.G. Harrison, Trans. Faraday Soc. **57**, 1191 (1961)
24. A.D. LeClaire, Br. J. Appl. Phys. **14**, 351 (1963)
25. J.D. Sirman, D. Waller, J.A. Kilner, in *Solid Oxide Fuel Cells V*, ed. by U. Stimming, S.C. Singhal, H. Tagawa, W. Lehnert (The Electrochemical Society, Pennington, NJ, 1997)
26. M. Kilo, Defect Diffus. Forum **242–244**, 185 (2005)
27. I. Kaur, Y. Mishin, W. Gust, *Fundamentals of Grain and Interphase Boundary Diffusion* (Wiley & Sons, West Sussex, 1995)
28. H.L. Tuller, J. Electroceram. **4**, 33 (1999)
29. J. Wolfenstine, P. Huang, A. Petric, J. Solid State Chem. **118**, 257 (1999)
30. M. Martin, Solid State Ion. **136–137**, 331 (2000)
31. C.D. Baertsch, K.F. Jensen, J.L. Hertz, H.L. Tuller, S.T. Vengallatore, S.M. Spearing, M.A. Schmidt, J. Mater. Res. **19** (9), 2604 (2004)
32. Z.P. Shao, S.M. Haile, J. Ahn, P.D. Ronney, Z.L. Zhan, S.A. Barnett, Nature **435**(7043), 795 (2005)
33. H.L. Tuller, A.S. Nowick, J. Phys. Chem. Solids **38**, 859 (1977)
34. K. Sasaki, J. Maier, J. Appl. Phys. **86**(10), 5422 (1999)
35. K. Sasaki, J. Maier, J. Appl. Phys. **86**(10), 5434 (1999)